Steel and Composite Structures, *Vol. 15, No. 3 (2013) 247-266*
DOI: http://dx.doi.org/10.12989/scs.2013.15.3.247

The behaviour of structures under fire – numerical model with experimental verification

Neno Torić*, Alen Harapin [a] and Ivica Boko [b]

University of Split, Faculty of Civil Engineering, Architecture and Geodesy, Matice Hrvatske 15, 21000 Split, Croatia

(Received October 07, 2011, Revised June 19, 2013, Accepted July 12, 2013)

Abstract. This paper presents a comparison of results obtained by a newly developed numerical model for predicting the behaviour of structures under fire with experimental study carried out on heated and simply supported steel beam elements. A newly developed numerical model consists of three submodels: 3D beam model designed for calculating the inner forces in the structure, 2D model designed for calculation of stress and strain distribution over the cross section, including the section stiffness, and 3D transient nonlinear heat transfer model that is capable of calculating the temperature distribution along the structure, and the distribution over the cross section as well. Predictions of the calculated temperatures and vertical deflections obtained by the numerical model are compared with the results of the inhouse experiment in which steel beam element under load was heated for 90 minutes.

Keywords: fire; numerical model; heat transfer; finite element; steel

1. Introduction

Behaviour of structures exposed to fire has been extensively studied through experimental research focused on the material behaviour (ECCS 1983, Anderberg 1983, Terro 1998, Youssef and Moftah 2007) and mechanical response of the structure under different types of boundary conditions and load levels (Wang *et al.* 1995, Elghazouli and Izzuddin 2000, El-Fitiany and Youssef 2009). Research regarding structure behaviour was mainly focused on the study of the behaviour of single span structures comprised of a single beam, or column, or combination of both. Studies have shown that the behaviour of building materials at high temperatures can be represented with elasto-plastic material model, with temperature dependent ultimate strength limit and modulus of elasticity. However, after reaching certain temperature extensive transient/creep deformations occur in material which affect the response of structures under fire, depending on the type of boundary conditions of the structure (Dwaikat and Kodur 2008, Wu and Lu 2009, Kodur and Dwaikat 2009). Conducted experimental studies enabled the development of different types of hybrid thermo-mechanical numerical models for predicting the behaviour of structures under fire.

*Corresponding author, Ph.D., E-mail: neno.toric@gradst.hr
[a] Professor, E-mail: alen.harapin@gradst.hr
[b] Professor, E-mail: ivica.boko@gradst.hr

http://www.techno-press.org/?journal=scs&subpage=8 ISSN: 1229-9367 (Print), 1598-6233 (Online)

Hybrid models were designed with various built-in formulations of the mechanical model of the structure, based on 1D/2D elements, to describe the geometry of the structure/cross-section, in combination with a 2D heat transfer model that gave predictions of temperature distribution over the cross-section during fire. A particular problem in experimental research that remained to define is a constitutive law of material's behaviour at high temperatures in multiaxial stress. This problem prevented the application of the full 3D mechanical model of the structure. The object of this paper is to demonstrate the capabilities of a newly developed hybrid thermo-mechanical model which incorporates 3D heat transfer model capable of taking into account the distribution of temperature along the element length and various types of boundary conditions on the structure surface.

2. The numerical model

2.1 Introduction

As it was previously noted, a numerical model that describes the behaviour of structures under fire must be able to describe, besides the nonlinear behaviour of structures under load, the development of temperature inside the structure and changes of the material parameters at high temperatures. A complete non-linear calculation must include the geometry of the cross-sections, the type and the distribution of the reinforcement (for reinforced concrete structures) and loading conditions, as well as the non-linear constitutive law of the materials' behaviour.

The results given by such a calculation can significantly change the image of the state of stresses and strains in a particular structural element, thus enabling the structural engineer to have a better insight into the behaviour, and possible failure of the load-bearing capacity of the structure.

2.2 The linear elastic model for beam elements

The common origin of almost all nonlinear analyses is linear analysis. The linear numerical model for frame structure analysis is well known and frequently described in literature (Prezeminiecki 1968, Bangash 1989), so we will only briefly note it here.

In this paper, two-node straight, ideally flat, in parts prismatic finite elements are used. Each element has 6 degrees of freedom in an each node, and they are the same ones that were used in a series of articles (Liew *et al.* 2000, Yang *et al.* 2002, Sapountzakis and Mokos 2007, Trogrlić and Mihanović 2008).

The problem can generally be described with a linear differential equation in the form

$$LDL\,p - Q^0 L\,p - f = 0 \tag{1}$$

where: Q is the vector of the internal forces, Q^0 is the couple force vector, f is the load vector, D is cross-section stiffness matrix which includes material and geometrical properties of the section and L is the differential operator.

One of the procedures most often used and most recognised for solving this differential equation is the Finite Element Method. The essence of this method is in replacing (simulating) the system with an unlimited number of degrees of freedom with a system that has a limited number of degrees of freedom. In order to achieve that, we presuppose (program) the behaviour of a

(unlimited) number of nodes of the system on one finite element, with the behaviour of a particular number of previously defined nodes on that same element.

The approximate solution for the displacements in one element assumes the form (Bangash 1989, Trogrlić *et al.* 2011)

$$p = \hat{p} = H\,u \tag{2}$$

where H is the matrix of base functions and u is the vector of unknown nodal displacements. The base (shape) functions are usually selected from the group Hermite's polynomials (Bangash 1989). From the equality of external and internal forces follows

$$u^T s + \int \hat{p}^T\, f\, dx = \int \varepsilon^T\, \sigma\, dx \tag{3}$$

i.e.

$$u^T s + \int u^T\, H^T f\, dx = \int u^T \left(B^T\, D\, B\right) u\, dx \tag{4}$$

and after multiplication of the left with u^T

$$s = \int \left(B^T\, D\, B\right) u\, dx - \int H^T f\, dx \tag{5}$$

or abbreviated

$$s^e = k^e\, u - F^e \tag{6}$$

where

s^e – the vector of internal forces at the ends of the finite element,
k^e – the element stiffness matrix,
F^e – the vector of external forces,
B – strain matrix which includes flexural and shear strain components

The element stiffness matrix and the element load vector, which are in the local coordinate system, have to be transformed to the global coordinate system. The balance of the global system is established by arranging the transformed element stiffness matrix and the element load vector in the global stiffness matrix and the global load vector.

$$K = \sum_e k_{gl}^e; \quad F = \sum_e F_{gl}^e \qquad K\,u = F \tag{7}$$

This is a well known expression, where K and F are the matrices of stiffness and loading, and u is the vector of global displacements. To solve the above equation it is necessary to introduce boundary conditions, which in the case of static problems are the given force and displacements at the edges of the system. The local stiffness matrix, before transformation, in explicit form can be written as

$$\mathbf{k}^e = \begin{bmatrix} \frac{EA}{\ell} & 0 & 0 & 0 & 0 & 0 & -\frac{EA}{\ell} & 0 & 0 & 0 & 0 & 0 \\ & \frac{12EI_z}{\ell^3} & 0 & 0 & 0 & \frac{6EI_z}{\ell^2} & 0 & -\frac{12EI_z}{\ell^3} & 0 & 0 & 0 & \frac{6EI_z}{\ell^2} \\ & & \frac{12EI_y}{\ell^3} & 0 & \frac{6EI_y}{\ell^2} & 0 & 0 & 0 & -\frac{12EI_y}{\ell^3} & 0 & \frac{6EI_y}{\ell^2} & 0 \\ & & & \frac{GI_x}{\ell} & 0 & 0 & 0 & 0 & 0 & \frac{GI_x}{\ell} & 0 & 0 \\ & & & & \frac{4EI_y}{\ell} & 0 & 0 & 0 & \frac{6EI_y}{\ell^2} & 0 & \frac{2EI_y}{\ell} & 0 \\ & & & & & \frac{4EI_z}{\ell} & 0 & \frac{6EI_z}{\ell^2} & 0 & 0 & 0 & \frac{2EI_z}{\ell} \\ & & & & & & \frac{EA}{\ell} & 0 & 0 & 0 & 0 & 0 \\ & & & & & & & \frac{12EI_z}{\ell^3} & 0 & 0 & 0 & -\frac{6EI_z}{\ell^2} \\ & & & & & & & & \frac{12EI_y}{\ell^3} & 0 & \frac{6EI_y}{\ell^2} & 0 \\ & & & & & & & & & \frac{GI_x}{\ell} & 0 & 0 \\ & & & & & & & & & & \frac{4EI_y}{\ell} & 0 \\ & & & & & & & & & & & \frac{4EI_z}{\ell} \end{bmatrix} \tag{8}$$

and it is clear that the local stiffness matrix, apart from depending on the beam length ℓ, also depends on the material parameters: E, G, and the geometrical parameters: A, I_y and I_z. On the real beam, on which load is applied, internal forces (moments) may cause changes of stress and strain distribution and changes in stiffness. By dividing the beam to sub-elements where each has its own real stiffness, materially nonlinear analysis can be easily implemented (Fig. 1).

Therefore, it is necessary to establish a procedure for calculating the stiffness of the cross-section under different levels of stress.

2.3 Non-linear analysis of the stress-strain state and stiffness of the cross-section

2.3.1 Basic assumptions

The model for determining the state of stress-strain and stiffness of the cross-section (Radnić and Harapin 1993) has the following basic assumptions.

- the sections remain straight after the deformation,
- there is no sliding at the connection of different materials after they are connected,
- the stress-strain relationship (constitutive law) is known for all materials.

2.3.2 The strain plane of the section

The graphical representation of the possible strain plane, with respect to the previous equilibrium state, is presented in Fig. 2. The additional strain $\Delta\varepsilon$ of the section point is defined by the plane equation

$$\Delta\varepsilon = \rho^T r \tag{9}$$

where

$$\rho^T = \left[\Delta\varepsilon_0, \rho_z, \rho_y\right] \tag{10}$$

$$r^T = \left[1, -y, z\right] \tag{11}$$

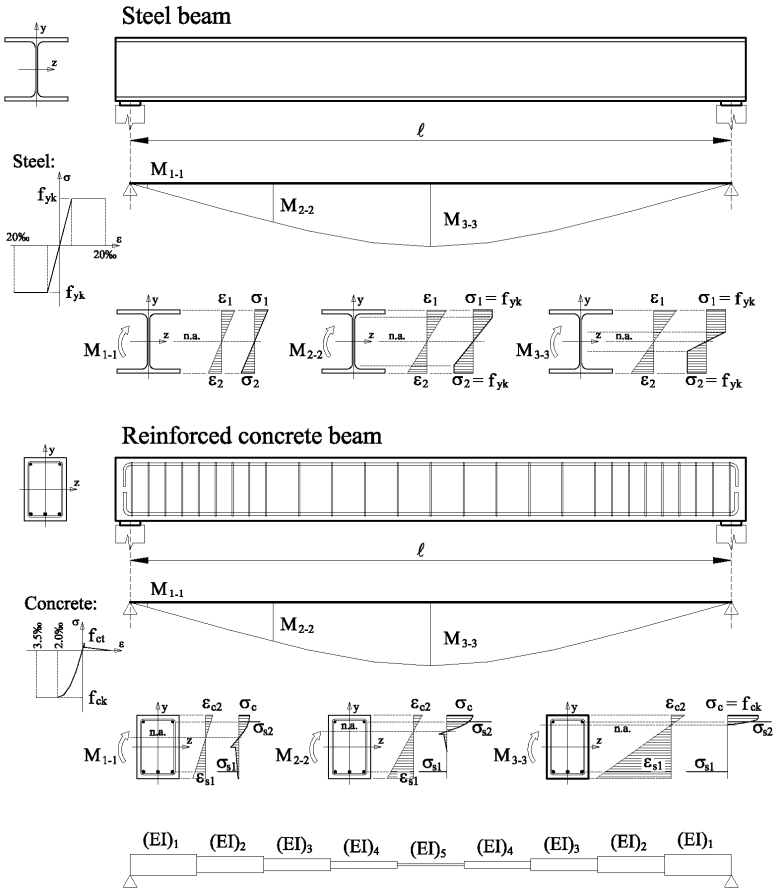

Fig. 1 The stress-strain state and stiffness along the girder according to the applied load

In the above expressions ρ represents the vector of unknown parameters of the additional strain plane, and y, z the coordinates of the point in the Y-Z plane. The strain plane is described by its intersection $\Delta\varepsilon_0$ with the X coordinate axis, and the components of relative rotations ρ_z, ρ_y about the Z and Y axis, respectively.

If the considered section point has previous strain ε_p, its total strain ε is

$$\varepsilon = \varepsilon_p + \Delta\varepsilon \tag{12}$$

Strain ε_p is known and determined by the previous equilibrium position ρ_p, i.e., analogous to Eq. (9) by

$$\varepsilon_p = \rho_p^T r; \quad \rho_p^T = \left[\varepsilon_{0p}, \rho_{zp}, \rho_{yp}\right] \tag{13}$$

If Eqs. (9)-(13) are introduced into Eq. (12), it follows

$$\varepsilon = \rho_p^T r + \rho^T r \tag{14}$$

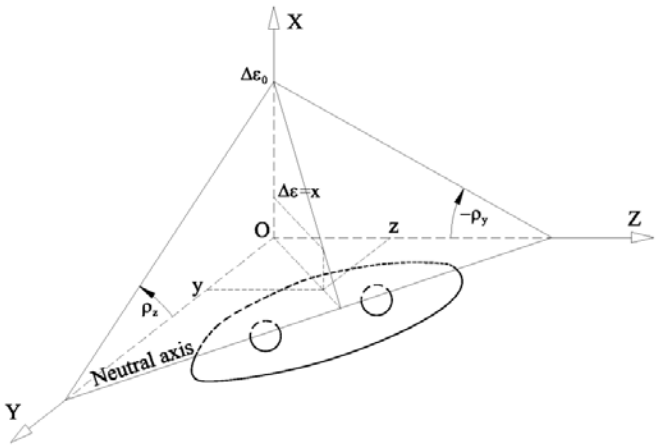

Fig. 2 Graphical representation of the possible strain plane

i.e.

$$\varepsilon = \rho_u^T r; \quad \rho_u = \rho_p + \rho \tag{15}$$

where ρ_u denotes the parameters of the total deformation plane.

2.3.3 The stress-strain relationship

The starting point for the stress-strain calculation procedure is the known relationship between the uniaxial stress σ and strain ε for each material. For real materials this relationship is essentially curvilinear, and it is determined by an uniaxial test or by the respective national codes. From the numerical analysis standpoint, it is appropriate to define this relationship as linear for each sector (Fig. 3). Thus, the introduced controlled error is negligible with regard to other assumptions. The stress-strain relationship between any of the two nodes i, j in the constitutive diagram is defined by

$$\sigma = \sigma_i + E(\varepsilon - \varepsilon_i) \tag{16}$$

If Eq. (14) is introduced into Eq. (16), and if substitution is introduced

$$\sigma' = \sigma_i\text{-}E\varepsilon_i + E\rho_p^T r \tag{17}$$

stress in the considered sector can be described by the following expression

$$\sigma = \sigma' + E\rho^T r \tag{18}$$

In the above expressions, E represents the modulus of elasticity (inclination of the line in the considered sector of $\sigma - \varepsilon$ diagram), whereas the graphical interpretation of stress σ' is presented in Fig. 3. For the known initial state, and the assumption of the current strain between nodes i, j is constant and determined.

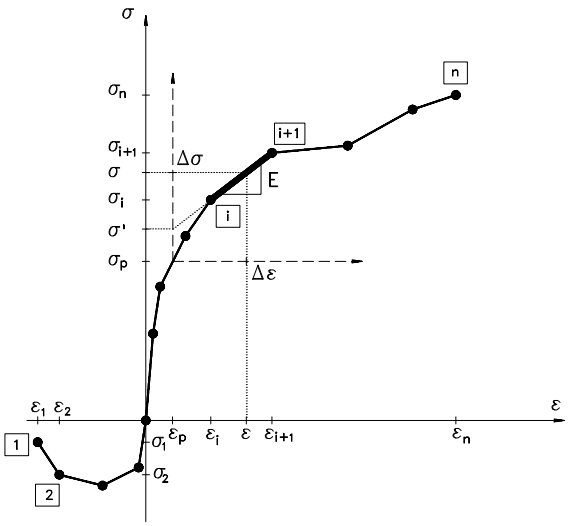

Fig. 3 Possible stress-strain relationship for a material

In the case of structure under fire, the stress-strain relationship of a material is temperature dependent. Because of that, the material behaviour under high temperatures is presented as a series of stress-strain curves determined at a specific temperature, with the linear interpolation of stress-strain values being used for temperatures in between.

2.3.4 The equilibrium equation

The vector of the internal resistance forces of the section S_u is the function of the resulting strain plane, and the $\sigma - \varepsilon$ relationship for a given material. If the resulting strain plane is known, S_u can be calculated by integration of the stresses in the section area. Thus

$$S_u = \left[N_u, M_{zu}, M_{yu}\right] = \sum_m \int_\Omega \sigma \, r d\Omega \tag{19}$$

where N_u represents the longitudinal internal force, M_{zu} and M_{yu} represent the force moments around the respective coordinate axes, Ω is the area of the given material and $\sum_m$ summation across all materials. If Eq. (18) is introduced into Eq. (19), it follows

$$S_u = S'_u + I\,\rho \tag{20}$$

where

$$S'_u = \sum_m \int_\Omega \sigma' \, r d\Omega \tag{21}$$

$$I = \sum_m \int_\Omega E r \, r^T d\Omega \tag{22}$$

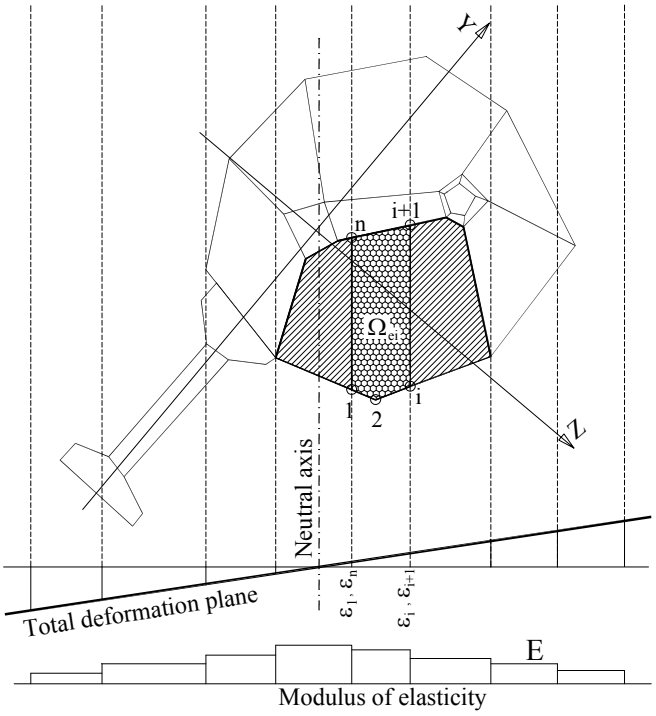

Fig. 4 Spatial discretization of the cross-section

S'_u represents one part of the vector of internal forces which is obtained by the integration of stresses σ'. The elements of the matrix I represent the current mechanical characteristics of the section, i.e., stiffness parameters. Vector S_v includes the vector of external forces S_{vp} which determines the initial strain plane ρ_p, and the vector of additional forces ΔS_v which causes additional strain plane ρ i.e.

$$S_v = S_{vp} + \Delta S_v \tag{23}$$

In order to achieve the equilibrium, S_v should be equal to S_u, i.e.

$$S_v - S_u = 0 \tag{24}$$

In the expanded form, Eq. (24) represents a system of three nonlinear equations with unknown $\rho^T = [\Delta\varepsilon_O, \rho_z, \rho_y]$.

2.3.5 Reinforcement bar

After determining the strain value of the considered reinforcement bar, it is used to determine between which nodal strains ε_i, ε_{i+1} it lies in the given $\sigma - \varepsilon$ diagram. Subsequently, it is possible to determine E and the contribution of the current mechanical characteristics of the bar materials, according to Eq. (22), by

$$I_s = \sum_s EA_s \, r \, r^T \tag{25}$$

where A_s represents the area of the bar under consideration, and $\sum_s$ summation across all the sectional bars. The part of the internal forces vector to which this reinforcement contributes, according to Eq. (21), is determined by

$$S'_{us} = \sum_s A_s \left(\sigma_i\text{-}E\varepsilon_i + E\varepsilon_p\right) r \tag{26}$$

As for the bar material, it is more appropriate to define the bar's initial strain by a discrete value ε_p, and not by ρ_p.

2.3.6 Material with a large area

Material, whose area is significant with regard to the whole cross-sectional area, is defined by convex polygonal elements without voids (FE). In the FE area there should be only one material (excluding the bar reinforcement). Each FE is defined by series of nodes and their coordinates, and by the material index. Consequently, the contours of each material are first approximated by a polygon, and then this area is divided into FE (Fig. 6). After determining the neutral axis position in the previous iteration, a set of lines is determined that are parallel to it. These lines connect FE points with strains equal to nodal strains ε_i of the $\sigma - \varepsilon$ diagram. Then, the intersection of these lines with the sides of each FE is sought, so, sub-elements with the constant E are defined. Matrix I_e for each of these sub-elements, with the following form

$$I_e = \begin{bmatrix} (A)_e & -(Q_z)_e & (Q_y)_e \\ -(Q_z)_e & (I_z)_e & (I_{zy})_e \\ (Q_y)_e & -(I_{zy})_e & (I_y)_e \end{bmatrix} \tag{27}$$

is obtained by summation across all the sides of the sub-element, according to the following equations

$$w_j = z_j \, y_{j+1}\text{-}z_{j+1} \, y_j \; ; \quad j = 1,2,3...n \; ; \quad n+1 = 1 \tag{28}$$

$$\begin{aligned}
(A)_e &= 1/2E \sum_m w_j \\
(Q_z)_e &= 1/6E \sum_m w_j \left(y_j + y_{j+1}\right) \\
(Q_y) &= 1/6E \sum_m w_j \left(z_j + z_{j+1}\right) \\
(I_z)_e &= 1/12E \sum_m w_j \left[\left(y_j + y_{j+1}\right)^2 - y_j y_{j+1}\right] \\
(I_y)_e &= 1/12E \sum_m w_j \left[\left(z_j + z_{j+1}\right)^2 - z_j z_{j+1}\right] \\
(I_{zy})_e &= 1/24E \sum_m w_j \left[\left(z_j + z_{j+1}\right)\left(y_j + y_{j+1}\right) + z_j y_j + z_{j+1} y_{j+1}\right]
\end{aligned} \tag{29}$$

where (z_j, y_j), (z_{j+1}, y_{j+1}) represent the boundary points coordinates of the considered sub-element side, and n the side number.

The summation is performed across all sides of the sub-element. Part of the vector S'_u to which this sub-element contributes, according to Eq. (20), is defined by

$$\left(S'_u\right)_e = \left(S'_{u1}\right)_e + \left(S'_{u2}\right)_e + I_e\,\rho_p \tag{30}$$

where

$$\left(S'_{u1}\right)_e = \int_{\Omega_e} \sigma_i\, r d\Omega = \begin{Bmatrix} \left(\overline{A}\right)_e \\ -\left(\overline{Q}_z\right)_e \\ \left(\overline{Q}_y\right)_e \end{Bmatrix} = \begin{Bmatrix} \left(\sigma_i/\varepsilon_i\right)\left(A\right)_e \\ -\left(\sigma_i/\varepsilon_i\right)\left(Q_z\right)_e \\ \left(\sigma_i/\varepsilon_i\right)\left(Q_y\right)_e \end{Bmatrix} \tag{31}$$

$$\left(S'_{u2}\right)_e = \int_{\Omega_e} \varepsilon_i\, E\, r d\Omega = \begin{Bmatrix} \left(\overline{\overline{A}}\right)_e \\ -\left(\overline{\overline{Q}}_z\right)_e \\ \left(\overline{\overline{Q}}_y\right)_e \end{Bmatrix} = \begin{Bmatrix} \varepsilon_i\left(A\right)_e \\ -\varepsilon_i\left(Q_z\right)_e \\ \varepsilon_i\left(Q_y\right)_e \end{Bmatrix} \tag{32}$$

The mechanical characteristics and one part of the internal force vector of one FE are obtained by summation of the respective characteristics of all sub-elements of that element. The same characteristics for each material are obtained by summation across all FE, which describe that material. Analogously, overall characteristics of the composite cross-section are obtained by performing summation across all materials.

2.4 The transient nonlinear heat transfer model

2.4.1 Differential equation

Transient heat transfer is a time-dependent process where the temperature field, created by heat transference inside the observed space, changes with time. The model that was developed and implemented is based on a 3D model of transient nonlinear heat transfer. The differential equation that describes this process in the spatial domain is defined by the equation

$$\rho C \frac{\partial T}{\partial t} = \frac{\partial}{\partial x_i} k_{ij} \frac{\partial T}{\partial x_j} + f \qquad i, j = 1,\ldots,3 \tag{33}$$

where

$\rho = \rho(x)$ – material density (kg/m^3),
$C = C(x,t)$ – specific heat capacity (J/kgK),
$k_{ij} = \rho C K_{ij}$ – the tensor of thermal conductivity coefficients (W/mK),
K_{ij} – the heat diffusion tensor (m^2/s).

By applying the weak formulation of the Eq. (33) and using Galerkin's method for selecting the function of the approximate solution, the system of p ordinary differential equations is obtained.

$$C_{mn}\frac{dT_m}{dt}+K_{mn}T_m=F_n+Q_n;\quad m,n=1,\ldots,p \tag{34}$$

where

$$C_{mn}=\int_{\Omega}\rho C\varphi_m\varphi_n d\Omega \tag{35}$$

$$K_{mn}=\int_{\Omega}k_{ij}\frac{\partial\varphi_m}{\partial x_i}\frac{\partial\varphi_n}{\partial x_i}d\Omega \tag{36}$$

$$F_n=\int_{\Omega}\varphi_n f d\Omega \tag{37}$$

$$Q_n=\int_{\Gamma}\varphi_n q d\Gamma \tag{38}$$

$$i,j=1,2,3;\quad m,n=1,\ldots,p$$

Ω – the spatial domain, Γ – the border of the spatial domain, φ_m, φ_n – base functions of the approximate solution, p – the total number of nodes in the spatial discretization.

The matrix C is the capacitance matrix, the matrix K is the conductance matrix, vector F is the internal heat source vector and Q is the heat flux vector. Heat flux caused by fire action consists of convection and radiation. The expression used to calculate the heat flux on the surface of the element can be defined as

$$q=\alpha_c\cdot(\theta_g-\theta_m)+\Phi\cdot\varepsilon_{res}\cdot\sigma\cdot(\theta_g^4-\theta_m^4) \tag{39}$$

where

q – surface heat flux (W/m^2), α_c – the convection coefficient (W/m^{2}K), Φ – the configuration factor, ε_{res} – the resultant emissivity factor between the element and the fire, σ – the Stephan Boltzmann's constant (=5.67*10^{-8} W/m^{2}K^4), θ_g – gas temperature in the vicinity of the element (°C), θ_m – surface temperature of the element (°C). The spatial domain is approximated by a suitable number of finite elements, according to Fig. 5. In the developed heat transfer model 8-node 3D finite elements are used.

2.4.2 The integration of discrete systems' equations

Nonlinear ordinary differential Eq. (34) are usually solved by integrating the equations between time steps for a relatively small time interval Δt. The temperatures at the beginning of the time interval (t) are known and used to calculate the temperatures at the end of the time interval, i.e., at time $t+\Delta t$. With an explicit-implicit (mixed) integration of the system of Eq. (34) the following expression is obtained

$$C_{mn}(T_m^{t+\Delta t}-T_m^T)+(1-\Theta)\Delta t(K_{mn}T_m^t-F_n^t-Q_n^t)+\Theta\Delta t(K_{mn}T_m^{t+\Delta t}-F_n^{t+\Delta t}-Q_n^{t+\Delta t})=0 \tag{40}$$

where

T_m^t – the vector of known temperature at the beginning of the time interval,

$T_m^{t+\Delta t}$ – the vector of unknown temperature at the end of the time interval

Θ – the interpolation parameter,
$F_n^{t+\Delta t}$ – the vector of heat source on the element at the end of the time interval,
$Q_n^{t+\Delta t}$ – the vector of boundary heat flow at the end of the time interval,
Δt – the incremental time step.

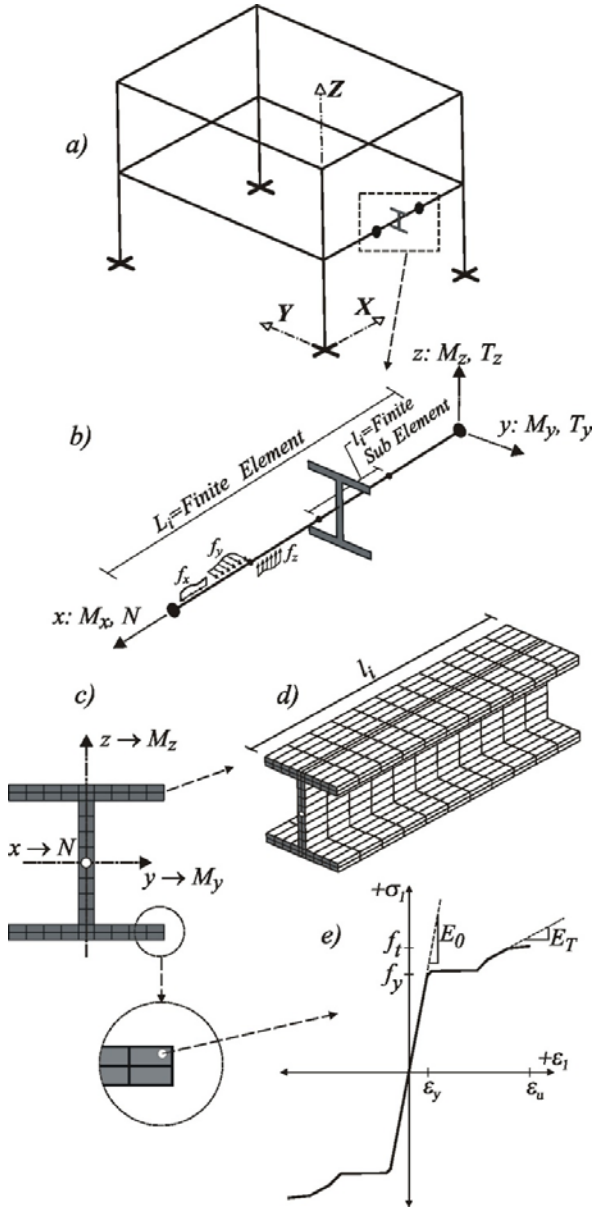

Fig. 5 (a) Global discretization of the space frame; (b) The beam-column element; (c) The element's cross-section discretization; (d) The comparative body model for heat transfer analysis; (e) The stress-strain constitutive law of the element's cross-section

The iterative procedure for determining the value $T_m^{t+\Delta t}$ starts with assuming the equation $T_m^{t+\Delta t} = T_m^t$ for the first iterative step within the time increment Δt. Then, for each iterative step, a new value for temperature at the end of the time interval is calculated, until the following condition is satisfied

$$\frac{\left\| T_m^{t+\Delta t} - T_m^t \right\|}{\left\| T_m^{t+\Delta t} \right\|} \leq \mu_p; \quad m = 1, \ldots, p \tag{41}$$

where: μ_p – the standard deviation.

2.5 *The complete nonlinear elastic model for predicting the behaviour of structures under fire*

Previously defined models: the model for analysis of linear-elastic beam systems, the model for transient nonlinear heat transfer and the model for dimensioning composite cross-sections have been combined into one integral model for analysis of materially nonlinear spatial beam systems under fire. The model was incorporated into the computer programme. Fig. 5 shows the discretization of one simple structure, on which the connection between the nodes that belong to the 2D mesh (used for discretization of the structure's cross-section) and the nodes that belong to the 3D mesh (used for spatial discretization of the structure's model for heat transfer) are presented.

It is necessary to define beginning and end points for each beam/column, as well as the cross-section with the constitutive law (the corresponding $\sigma - \varepsilon$ diagram) for every used material. The 3D spatial finite element mesh is then automatically generated along the beam/column. Before calculating the stress and stiffness on the cross section's finite element, the mean (average) temperature of the corresponding 3D finite element used in heat transfer model is calculated. Constitutive law of the material is then modified in accordance with the mean temperature, and the state of stress and stiffness of the section is determined.

It starts from the cross-section's zero-state level by calculating the real stiffness of the cross-section, according to Eq. (22), i.e., Eqs. (25)-(27). The calculated parameters present members of the starting stiffness matrix (8). It is important to say that the integration on the sectional level helps adjust/correct the axial, shear and bending sectional characteristics, while the torsion features remain unchanged. What follows is the usual procedure of arranging the global stiffness matrix and the global load vector (7).

After calculating the internal forces at the ends of the beam, the new strain plane position and the new stiffness of the section are determined. Generally, two cases are possible:

(1) It is possible to determine the strain plane position of the section. In this case the section is strong enough to withstand the external force influence (i.e. force resulting from the linear analysis of the beam system).
(2) It is not possible to determine the strain plane position of the section, i.e. the procedure shown in part 2.2 diverges. In this case, it is stated that what happened is the break of the section, i.e., the local break in the system, as well as the possible global break of the system.

The procedure continues as long as the build-up displacement vector falls under the optionally chosen small value, i.e.

Table 1 The numerical model of the incremental procedure

[1]	Defining the null force vector ($F = 0$); from it defining the starting parameters of the local stiffness matrix for every beam/column (25) and (27) and from them the local matrices of stiffness (8) as well as the starting global matrix of stiffness K_0 (7) $K_0 = \sum_e k^e_{gl,0}$ This is the null-stiffness, the stiffness of the system on which no forces are applied.
[2]	From the given external load on the beams/columns, defining the forces on elements, and the vector of the applied forces $F^e = \int H^T f \, dx; \quad F^e_{gl} = T \, F^e; \quad F = \sum_e F^e_{gl}$
[3]	The time loop (first time step j=1) is set.
[4]	The calculation of the temperature field in the 3D element (Fig. 5). Follow the calculation of the mean temperature and the correction of the material characteristics according to the calculated mean temperature for each cross section. $\rho C \frac{\partial T}{\partial t} = \frac{\partial}{\partial x_i} k_{ij} \frac{\partial T}{\partial x_j} + f \qquad i, j = 1,\ldots,3$
[5]	The incremental loop (first incremental step $i = 1$) is set.
[6]	The calculation of the nodes' displacements, and internal forces in elements: $K_i \, u_i = F \;\Rightarrow\; u_i = K_i^{-1} F; \;\; u_i = \{u_i, v_{pi}, w_{pi}, \theta_i, w_{si}, v_{si}\}$ $s^e = k^e u - F^e$
[7]	Convergence control: $\Delta u_i = u_i - u_{i-1} \qquad \frac{\lVert \Delta u_i \rVert}{\lVert u_i \rVert} \le \mu_p$ If the convergence is satisfied, the procedure is finished and the results are printed. Procedure continues with new time step: $j = j + 1$. If the convergence is not satisfied, the procedure continues – step [8]. The value μ_p is an optionally chosen small value, usually 0.001.
[8]	The calculation of the new stiffness in 2D elements, according to corrected material characteristics and the corrected internal forces. $K_i = I = I_e + I_s = \sum_m \int_\Omega E r \, r^T \, d\Omega \quad \text{“+”} \quad \sum_s E \, A_s r \, r^T$ Procedure continues on step [6].

$$\frac{\lVert \Delta u_i \rVert}{\lVert u_i \rVert} \le \mu_p \tag{42}$$

In all practical cases, the value μ_p can be chosen as 0.001. Incremental calculation procedure as well as the flowchart of the computer program is presented in Table 1 and Fig. 6.

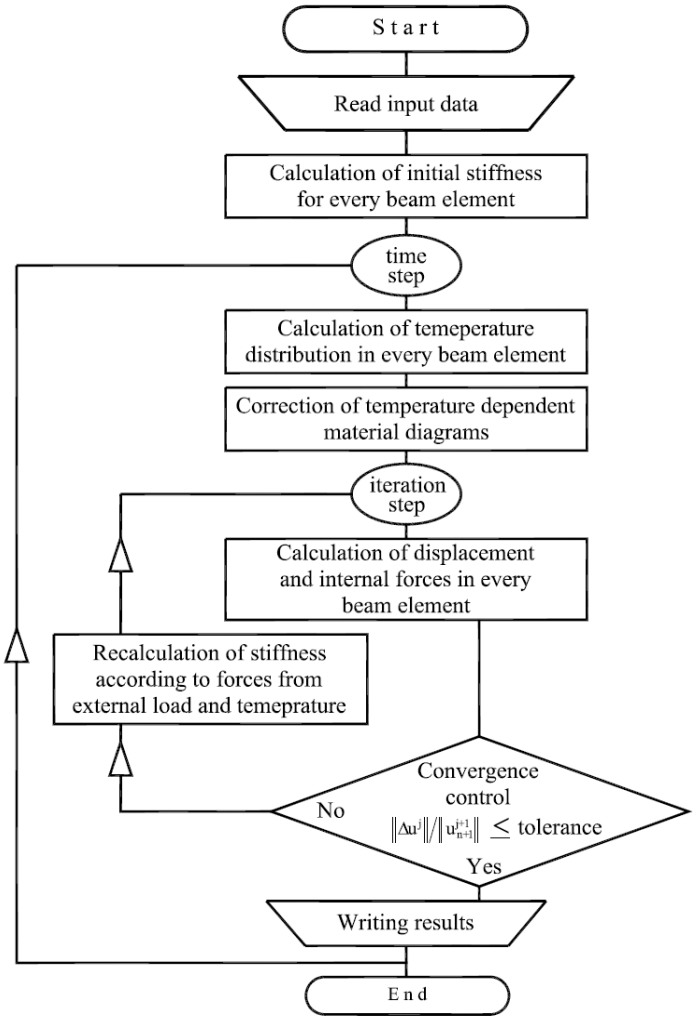

Fig. 6 Flowchart of the computer programme

3. Example of numerical modelling of steel beam under high temperatures

This chapter describes a comparison of results made between the predictions of the model and the results obtained by inhouse experiment (Boko *et al.* 2007). A simply supported welded steel beam I 212/180, steel grade S355J2G3 with a total length of 2.5 m was previously loaded by a concentrated force of 200 kN at midspan. Afterwards, the beam was heated by increased temperature gradient of 5°C/min for 90 minutes, while only a part of the beam was positioned inside the furnace. During the experiment, surface temperatures and midspan deflection were measured in discrete points on the element surface. Fig. 7 presents the experimental setup along with the disposition of the measuring points on the element.

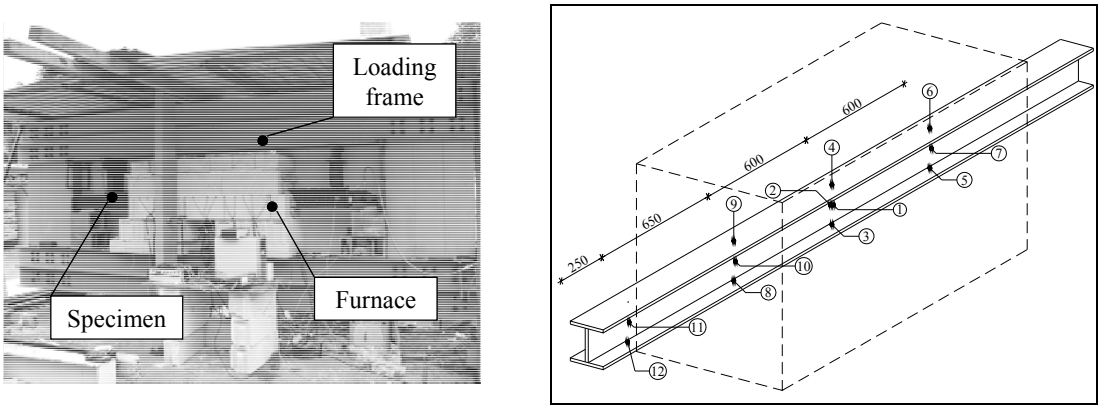

Fig. 7 The experimental specimen (Boko *et al*. 2007) with the disposition of the temperature measuring points

Table 2 Section dimensions and characteristics

Depth (mm)	Width (mm)	Web thick (mm)	Flange thick (mm)	Moment of inertia (cm^4)		Area (cm^2)
				Axis xx	Axis yy	
212.0	180.0	16.0	16.0	5929.0	1460.0	84.5

Table 3 Basic heat transfer input parameters

Thermal conductivity λ	Specific heat capacity C	ρ_a (kg/m^3)	α_c (W/m^{2}K)	Φ	ε_{res}	Δt (s)
EN1993-1-2	EN1993-1-2	7850.0	25.0	1.0	0.7	0.5

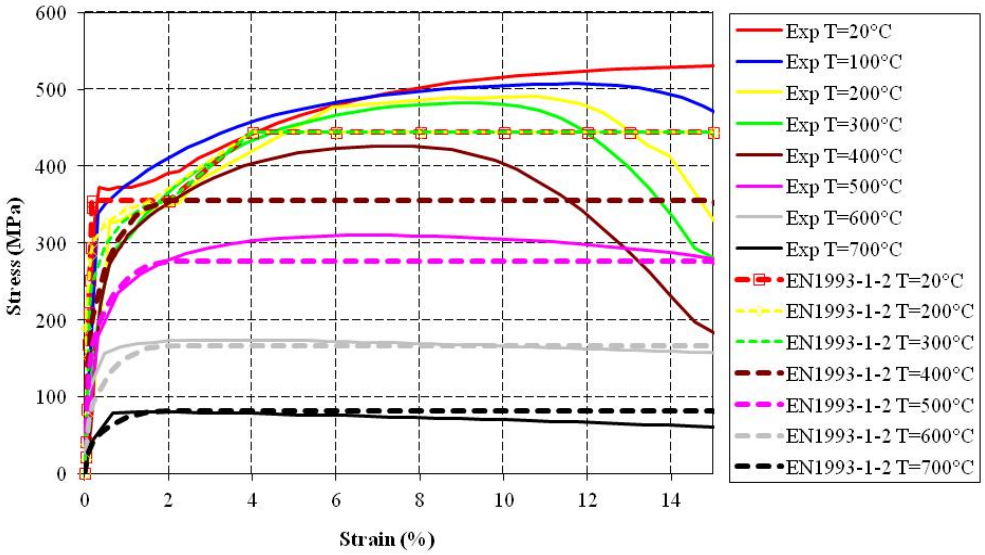

Fig. 8 Temperature dependent stress-strain curves obtained by the experiment and taken from EN1993-1-2

The dimensions and the geometrical characteristics of the analyzed cross-section are given in Table 2.

An example of modelling the behaviour of a simply supported steel beam under fire was analyzed for two different types of input stress-strain mechanical characteristics: experimentally

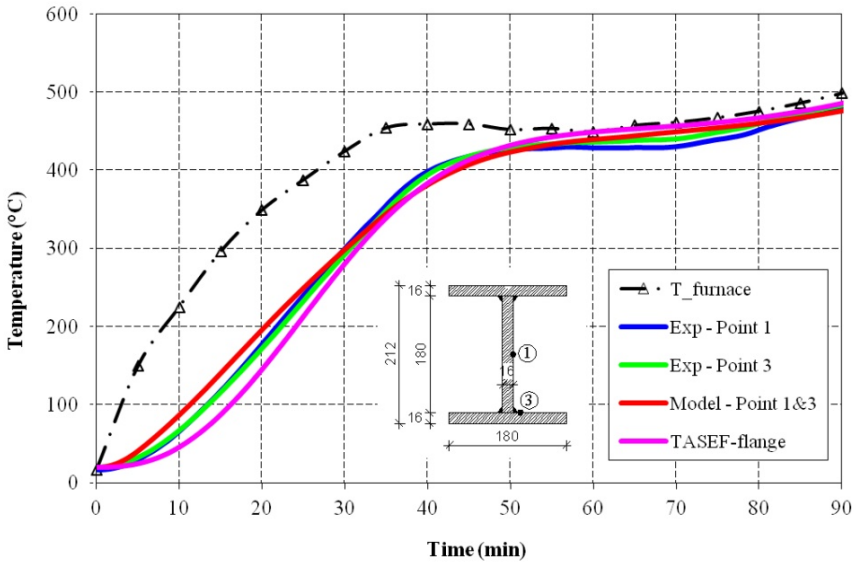

Fig. 9 The comparison of the results of the developed temperatures between the experiment and model predictions – lower flange and web (1.25 m)

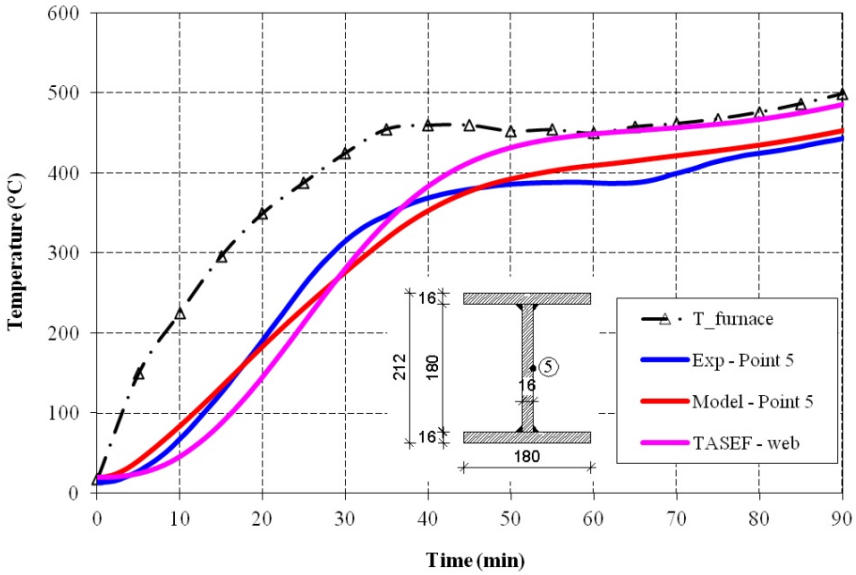

Fig. 10 The comparison of the results of the developed temperatures between the experiment and model predictions – web (1.85 m)

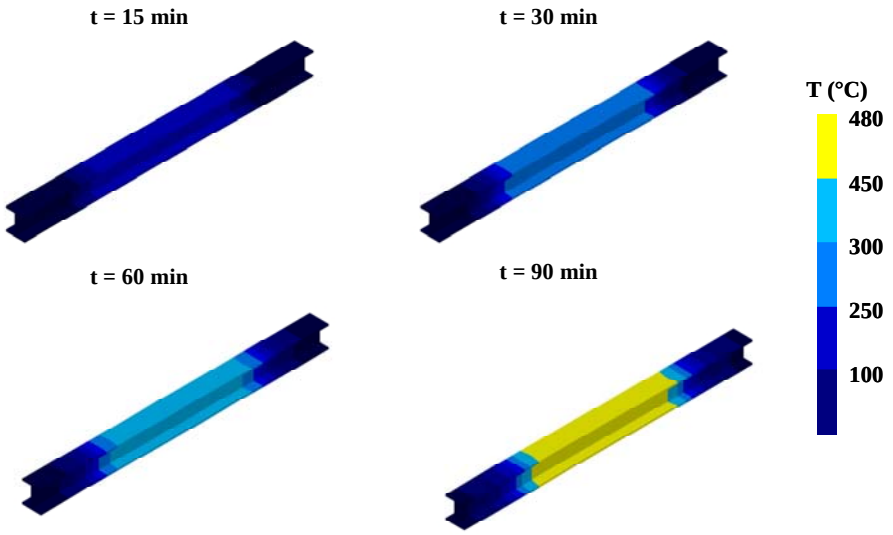

Fig. 11 The evolution of the temperature field in discrete time intervals across the steel element

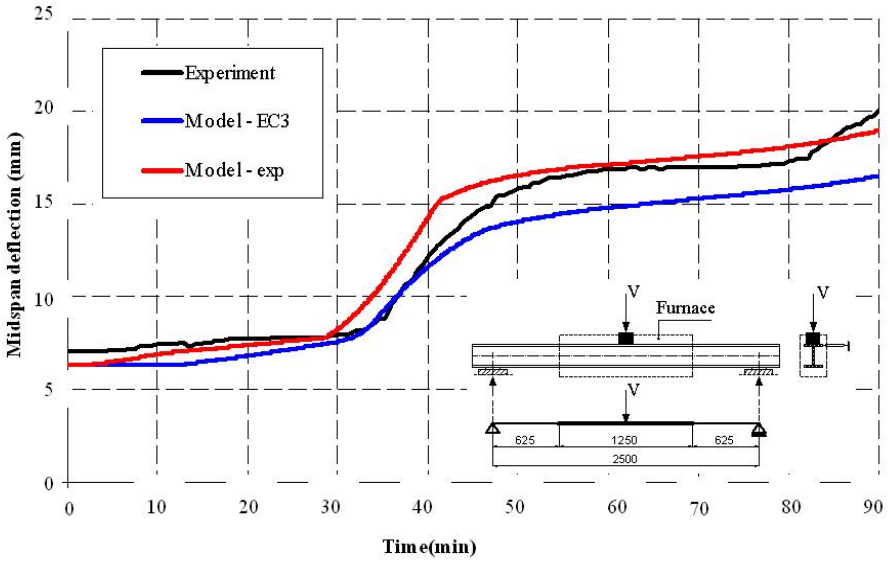

Fig. 12 The comparison of the results of vertical deflections between the experiment and the model predictions for two different types of stress-strain curves

determined stress-strain curves (Boko *et al.* 2007) which were determined by testing stationary heated specimens of steel that was used in the steel beam itself and the stress-strain curves proposed by EN1993-1-2 2005, generally used for engineering analysis of the behaviour of steel structures under fire. Steady-state heating method was used for heating the specimens in series of two specimens for each temperature level. In the steady-state heating method, after having been heated to a predetermined temperature level, the specimen was loaded with a strain increase of

0.02%/sec. The strain increase in the specimen was measured with the help of video-extensometer. The stress-strain curves used in the example are plotted in Fig. 8.

Figs. 9, 10 and 11 show the comparison between the results of the measured temperatures taken from the experiment and the temperatures calculated by the proposed model in the discrete points of the beam element. Additionally, the heat transfer analysis over the cross-section has been performed by using 2D heat transfer model TASEF (Sterner and Wickstrőm 1990) for comparison.

Fig. 12 shows the comparison between the results of measured vertical deflections at midspan taken from the experimental data and the predictions of the model for two different types of input stress-strain curves.

3.1 Discussion of results

- Fig. 9 proves that the predictions of temperatures calculated by the 3D heat transfer model are fairly accurate, with some discrepancy in the temperature prediction occurring at the end of the furnace (Fig. 10),
- The usage of 3D model, rather than TASEF, yields better results in the prediction of the temperature spread after 40 minutes, as it is shown by the Fig. 10.
- Fig. 12 shows that the prediction of vertical deflections calculated by the model in the first 85 minutes was quite correct. A large discrepancy that occurs afterwards, at temperatures above 450°C, is accounted for by the phenomenon of steel creep. The phenomenon can highly affect steel deformation, however, it was not taken into account by the proposed model,
- Fig. 12 also shows a small discrepancy observed with respect to vertical deflections between two different sets of stress-strain curves, with the predictions of deflections using EC3 curves on the unsafe side.

4. Conclusions

Verification of a newly developed hybrid thermo-mechanical model has shown the ability of the model to accurately predict the temperature field and the stiffness reduction of partially heated steel elements, which is possible only by coupling 3D heat transfer model with the structural analysis model. The main benefits of the proposed model combination is the accurate prediction of temperature field and stiffness reduction in case when structural parts are not heated uniformly, which is a common property for steel columns in fires or for steel beams in case of a localized fire. The major limitation of the proposed model is the fact that, in case of analyizing the whole structure behaviour, large number of finite elements for heat transfer analysis has to be employed.

5. Further research

- Further research will be based on the implementation of implicit and explicit steel creep models in order to improve predictions of the proposed model with regard to vertical deflections.
- Abilities of the heat transfer model with regards to various boundary conditions on the structure surface will be tested in future experimental research.
- Future work will also focus on the enhancement of capabilities of the proposed model to

predict the behaviour of statically indeterminate structures under fire.

References

Anderberg, Y. (1983), *Properties of Materials at High Temperatures – Steel*, RILEM Report, University of Lund, Sweden

Bangash, M.J.H. (1989), *Concrete, Concrete Structures, Numerical Modelling, Applications*, Elsevier Applied Science, New York, NY, USA.

Boko, I., Peroš, B. and Torić, N. (2007), "Fire Resistance Determination of Steel Structures", *Proceedings of 3rd International Conference on Structural Engineering, Mechanics and Computation*, Cape Town, South Africa, September.

Dwaikat, M.B. and Kodur, V.K.R. (2008), "A numerical approach for modelling the fire induced restraint effects in reinforced concrete beams", *Fire Safety J*., **43**(4), 298-307.

ECCS Technical Committee 3 (1983), *European Recommendations for the Fire Safety of Steel Structures, Calculation of the Fire Resistance of Load Bearing Elements and Structural Assemblies Exposed to the Standard Fire*, Amsterdam, Elsevier Scientific Publishing Company.

El-Fitiany, S.F. and Youssef, M.A. (2009), "Assessing the flexural and axial behaviour of reinforced concrete members at elevated temperatures using sectional analysis", *Fire Safety J*., **44**(5), 691-703.

Elghazouli, A.Y. and Izzuddin, B.A. (2000), "Response of idealized composite beam-slab systems under fire conditions", *J. Construct. Steel Res*., **56**(3), 199-224.

EN 1993-1-2:2005 (2005), *Eurocode 3 - Design of steel structures - Part 1-2: General Rules - Structural fire design*, European Committee for Standardization, Brussels.

Kodur, V.K.R. and Dwaikat, M.M.S. (2009), "Response of steel beam-columns exposed to fire", *Eng. Struct*., **31**(2), 369-379.

Liew, J.Y.R., Chen, W.F. and Chen, H. (2000), "Advanced inelastic analysis of frame structures", *J. Construct. Steel Res*., **55**(1-3), 245-265.

Prezeminiecki, J.S. (1968), *Theory of Matrix Structural Analysis*, McGraw-Hill, New York, NY, USA.

Radnić, J. and Harapin, A. (1993), "Model dimenzioniranja kompozitnih poprečnih presjeka", *Građevinar*, **45**(7), 379-389.

Sapountzakis, E.J. and Mokos, V.G. (2007), "3-D beam element of composite cross section including warping and shear deformation effects", *Comput. Struct*., **85**(1-2), 102-116.

Sterner, E. and Wickstrőm U. (1990), *TASEF-Temperature Analysis of Structures Exposed to Fire*, Swedish National Testing Institute.

Terro, M.J. (1998), "Numerical modeling of the behaviour of concrete structures in fire", *ACI Struct. J*., **95**(2), 183-193.

Trogrlić, B. and Mihanović, A. (2008), "The comparative body model in material and geometric nonlinear analysis of space R/C frames", *Eng. Comput*., **25**(2), 155-171.

Trogrlić, B., Harapin, A. and Mihanović, A. (2011), "The null configuration model in limit load analysis of steel space frames", *Materialwissenschaft und Werkstofftechnik*, **42**(5), 417-428.

Wang, Y.C., Lennon, T. and Moore, D.B. (1995), "The behaviour of steel frames subject to fire", *J. Construct. Steel Res*., **35**(3), 291-322.

Wu, B. and Lu, J.Z. (2009), "A numerical study of the behaviour of restrained RC beams at elevated temperatures", *Fire Safety J*., **44**(4), 522-531.

Yang, Y.B., Kuo, S.R. and Wu Y.S. (2002), "Incrementally small-deformation theory for nonlinear analysis of structural frames", *Eng. Struct*., **24**(6), 783-798.

Youssef, M.A. and Moftah, M. (2007), "General stress-strain relationship for concrete at elevated temperatures", *Eng. Struct*., **29**(10), 2618-2634.

CC